East European Journal of Physics. 3. 681-688 (2026)
DOI:10.26565/2312-4334-2026-3-64 ISSN 2312-4334

STOICHIOMETRIC EVOLUTION OF MULTI-PHASE TUNGSTEN NITRIDES UNDER VARIABLE GAS FLOW AND AUXILIARY PLASMA ASSISTANCE DURING MAGNETRON SPUTTERING[G]

O.V. Maksakova*, V.M. Beresnev, I.M. Sereda, Ya.O. Hrechko, A.O. Skrypnyk, S.I. Bogatyrenko, S.V. Lytovchenko, B.O. Mazilin
V.N. Karazin Kharkiv National University, 4, Svoboby Sq., 61000 Kharkiv, Ukraine
**Corresponding author email: o.maksakova@karazin.ua*
Received _June 31, 2026; revised August 5, accepted August 15, 2026

In this work, the influence of Ar/N_2 gas mixture composition and auxiliary plasma-assisted activation on the structural-phase evolution of tungsten nitride (WN) coatings deposited via planar magnetron sputtering was systematically investigated. The coatings were synthesized using a 100-mm diameter tungsten target under varying reactive gas regimes (from 50% to 10% N_2) and two electrical configurations: an additional biased anode (+200 V) and a standard grounded anode setup. X-ray diffraction coupled with qualitative and quantitative optimization proved that the coatings possess a complex heterophase structure composed of hexagonal hcp-WN and cubic fcc-W_2N phases. It has been established that the persistent dominance of the hcp-WN phase with a highly stable (111) texture acts as a rigid energetically favored framework across all gas flow ratios. Decreasing the nitrogen content primarily affects the secondary, more compliant cubic phase component. At a critical nitrogen deficiency of 10%, the growth of the preferred (200) cubic planes becomes heavily suppressed, forcing the matrix towards grain refinement (nanocrystallization) and stimulating the structural integration of mixed-phase (220)fcc + (102)hcp configuration. Furthermore, shifting to the grounded anode configuration collapses the auxiliary glow discharge zone, dropping the near-substrate plasma density from 7.5×10^{10} cm^{-3} to 4×10^{10} cm^{-3}. The resulting reduction in adatom surface diffusion length causes rapid thermal quenching, leading to complete texture randomization, a sharp fourfold increase in the isotropic (111)fcc + (100)hcp reflection, and the accumulation of structurally imperfect phase boundaries. The application of an auxiliary biased anode serves as an effective tool to decouple the destructive effects of high-energy ion bombardment from the beneficial structural ordering induced by high-flux, low-energy plasma activation.
Keywords: *Magnetron Sputtering; Nitrides; Tungsten; XRD; Phase; Structure; Gas flow*

INTRODUCTION

Transition-metal nitrides, particularly tungsten nitrides, have garnered significant academic and industrial interest owing to their exceptional mechanical hardness, high thermal stability, remarkable wear resistance, and reliable chemical inertness [1-5]. These properties make them highly attractive for a wide range of cutting-edge applications, including diffusion barriers in microelectronics, protective coatings for high-temperature machining tools, and active components in catalytic energy conversion systems [6-10]. In the field of surface engineering, magnetron sputtering stands out as the premier deposition technique for synthesizing such thin films due to its excellent scalability, high reproducibility, and capability to deposit dense, adherent coatings at relatively low substrate temperatures [11-13].

However, the deterministic synthesis of multi-phase tungsten nitride coatings remains a complex materials science challenge. Unlike other transition metal nitrides, the W-N system exhibits a rich and complex phase diagram comprising several distinct structural configurations, primarily the hexagonal hcp-WN and cubic fcc-W_2N phases [14-15]. The competitive nucleation and spatial orientation of these phases are heavily dictated by the thermodynamic driving forces of chemical reactions at the substrate and the kinetic energy transfer to the growing film interface. Consequently, precise control over the structural-phase evolution and texturing is essential, as the final performance of the coating is inherently linked to its precise phase boundary configuration and grain orientation.

To systematically optimize the performance of the WN coatings, two critical deposition parameters can be comprehensively evaluated. The first one is a reactive gas mixture composition (i.e. Ar/N_2 flow ratio). This parameter directly regulates the chemical stoichiometry and nitrogen saturation degree of the tungsten lattice [16-17]. A precise balance of the reactive gas is critical to avoid either a total collapse of the stoichiometric crystalline phase or severe target poisoning during the sputtering process. The second one is a low-energy ion bombardment kinetics. Controlling the plasma parameters at the growth front is paramount for modulating film density, grain size, and texture crystallization [16-17]. Traditional methods often rely on high negative substrate bias voltages to accelerate ions; however, this approach frequently induces high intrinsic macrostrains, atomic displacement, and destructive lattice defects.

To overcome these structural limitations, auxiliary plasma assistance via an additional biased anode emerges as a crucial engineering tool for magnetron sputtering. This configuration enables an effective decoupling of the destructive high-energy ion impacts from the highly beneficial structural ordering driven by a high-flux, low-energy plasma activation. By effectively doubling the local plasma density without altering the safe ion impact energy threshold, the

Cite as: O.V. Maksakova, V.M. Beresnev, I.M. Sereda, Ya.O. Hrechko, A.O. Skrypnyk, S.I. Bogatyrenko, S.V. Lytovchenko, B.O. Mazilin, East Eur. J. Phys. 3, 681 (2026), https://doi.org/10.26565/2312-4334-2026-3-64

auxiliary anode dramatically accelerates the lateral surface diffusion of arriving adatoms, allowing the system to easily overcome local potential barriers and crystallize into thermodynamically preferred textures.

While separate studies have addressed either gas flow dynamics or plasma assistance [18-19], a systematic understanding of their synergistic influence on the phase transition kinetics of heterophase WN/W_2N nanocomposite systems remains insufficient.

The aim of this work is to systematically investigate the combined effects of the Ar/N_2 gas flow ratio and auxiliary biased anode configuration on the stoichiometric evolution, and phase boundary perfection of multi-phase tungsten nitride coatings deposited via reactive magnetron sputtering.

EXPERIMENTAL DETAILS

Deposition

A planar magnetron sputtering system equipped with a 100-mm diameter tungsten target and an additional anode was employed for the deposition of WN and WC coatings (see Figure 1). Prior to deposition, the vacuum chamber was evacuated using a turbomolecular pump to a base pressure of approximately 5×10^{-5} Torr. For the WN deposition, high-purity argon and nitrogen were introduced into the chamber at different Ar/N_2 flow-rate ratios. The total working pressure was maintained at approximately 9×10^{-4} Torr.

The magnetron was operated with a 100 Hz sinusoidal voltage waveform, with a peak cathode voltage of approximately 450 V and a peak discharge current of approximately 1.5 A. An additional anode was biased at approximately +200 V to generate an additional glow-discharge plasma in the region between the magnetron and the substrate. The substrate was positioned at a distance of 140 mm from the target and was electrically insulated during deposition. Under the deposition conditions, the ion energy incident on the substrate, measured using a retarding-field analyzer (RFA), was approximately (10 ÷ 12) eV with respect to substrate floating potential. Plasma density measured with Langmuir probe near the substrate was approximately 7.5×10^{10} cm^{-3} with electron temperature of about 2 eV.

The deposition time was fixed at 30 min for all experiments. The coating thickness was monitored using a quartz crystal microbalance and was approximately 500 nm for the WN coatings.

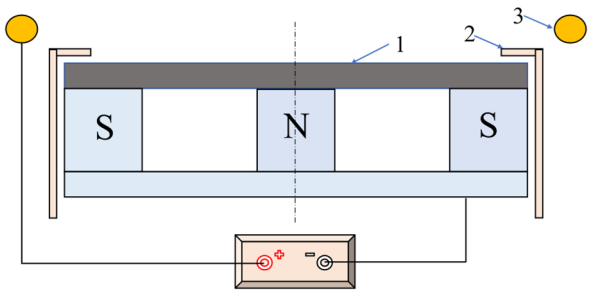

Figure 1. The scheme of experimental device: 1 – tungsten target; 2 – insulated cylinder; 3 – anode

For the deposition of WN coatings at different gas regimes, a precise gas mixing procedure based on partial pressure management was implemented. The total working pressure within the vacuum chamber was strictly maintained at a constant value of approximately 9×10^{-4} Torr, which was defined as 100% of the total gas volume. Prior to the introduction of the reactive gas, high-purity argon (Ar) was admitted into the chamber via a dedicated piezoceramic leak valve until its partial pressure reached the specific required percentage of the total working pressure (i.e., 50%, 70%, 80%, or 90%, respectively). Subsequently, high-purity nitrogen (N_2) was introduced through a separate independent leak valve to act as the reactive gas, adjusting the total pressure upward until the final working threshold of 9×10^{-4} Torr was precisely achieved. This sequential gas-feeding method ensured highly reproducible Ar/N_2 flow-rate ratios, corresponding to discrete concentrations of 50%, 30%, 20%, and 10% of N_2 in the plasma volume.

For the comparative study, a series of WN coatings was also deposited under the conventional magnetron sputtering configuration, where the additional anode was kept at the ground potential (referred to as the “grounded anode” mode). This setup represents the standard operating regime of the magnetron system without the generation of an auxiliary plasma enhancement zone. Under these conditions, the plasma density measured with the Langmuir probe in the vicinity of the substrate dropped by approximately a factor of two, yielding a value of 4×10^{10} cm^{-3}. Despite the significant decrease in plasma density, the average energy of the ions incident on the substrate surface remained practically unaltered at approximately 12 eV. All other deposition variables, including the target-to-substrate distance, working gas pressure (80 Ar / 20 N_2), and total deposition time, were maintained identical to those utilized in the biased anode experiments to ensure a direct comparison of the structural-phase evolution.

The crystal structure, phase composition, and substructural characteristics of the WN coatings were evaluated by X-ray diffraction (XRD). The XRD measurements were performed on a diffractometer utilizing a Cu-Kα radiation source (λ = 1.540600 Å) operating at an accelerating voltage of 30.0 kV and a tube current of 30.0 mA. The optical configuration of the goniometer included a 1.0° divergence slit, a 1.0° scatter slit, and a 0.15 mm receiving slit. The diffraction patterns were recorded in the theta–2theta coupled scanning mode over a 2theta angular range of 10.0°–100.0° with a step size (sampling pitch) of 0.02° and a continuous scanning speed of 2.000°/min.

Phase identification and qualitative/quantitative analysis were carried out using the Match! phase analysis software package (Crystal Impact, Bonn, Germany), coupled with the PDF-2 (Release 2004) reference database. Quantitative phase evaluation was performed via the Reference Intensity Ratio (RIR) method based on integrated profile areas. The experimental diffraction data was smoothed prior to analysis without subtracting the background or the α2 radiation component.

According to the quantitative search-match optimization, the matrix consists of a complex multi-phase nitride system dominated by two major tungsten nitride phases: a hexagonal hcp-WN phase (space group P6̄m2, lattice parameters a = 2.89 Å and c = 2.83 Å, entry No. 03-065-9410) and a cubic fcc-WN phase (space group Fm3̄m, lattice parameter a = 4.126 Å, entry No. 00-025-1257).

EXPERIMENTAL RESULTS

Structural-phase analysis at standard configuration

Figure 2 illustrates the X-ray diffraction patterns of the WN coatings deposited via magnetron sputtering under various working gas flow ratios (Ar/N_2). The corresponding substructural and phase parameters calculated from the diffraction peak profiles are summarized in Table 1.

A detailed analysis of the phase composition of individual samples revealed the important trends.

For the WN (50 Ar / 50 N_2) coating, at the maximum concentration of the reactive gas (nitrogen) in the deposition chamber, a heterophase structure is formed, consisting of a dominant hexagonal phase hcp-WN and a cubic phase fcc-W_2N. The XRD pattern exhibits a low-intensity, broadened peak at 2theta = 35.98°, corresponding to the superposition of the (111)fcc + (100)hcp planes. The main contribution to the diffraction pattern comes from the peaks at 2theta = 42.95° the (200)fcc-W_2N plane, relative intensity I/I_0 = 562.88 a.u. and 2theta = 73.36° (111)hcp-WN. The latter exhibits the maximum intensity 1000.00 a.u., indicating the formation of a pronounced axial growth texture of the hexagonal phase. A (400)fcc-W_2N peak is also detected at higher angles 2theta = 88.90°.

For the WN (70 Ar / 30 N_2) coating, the reducing the nitrogen content to 30% does not lead to a qualitative rearrangement of the crystal lattice; however, it activates structural ordering processes. The combined peak around 2theta = 35.38° becomes more pronounced I/I_0 = 63.59 a.u., (FWHM = 1.2800). A moderate increase in intensity for the (200)fcc-W_2N plane to I/I_0 = 644.97 a.u. is observed, while the full width at half maximum (FWHM) broadens slightly to 0.4000, which may indicate the generation of local microstrains due to changes in the stoichiometric coefficient. The texture of (111)hcp-WN at 2theta = 73.24° retains its dominant position.

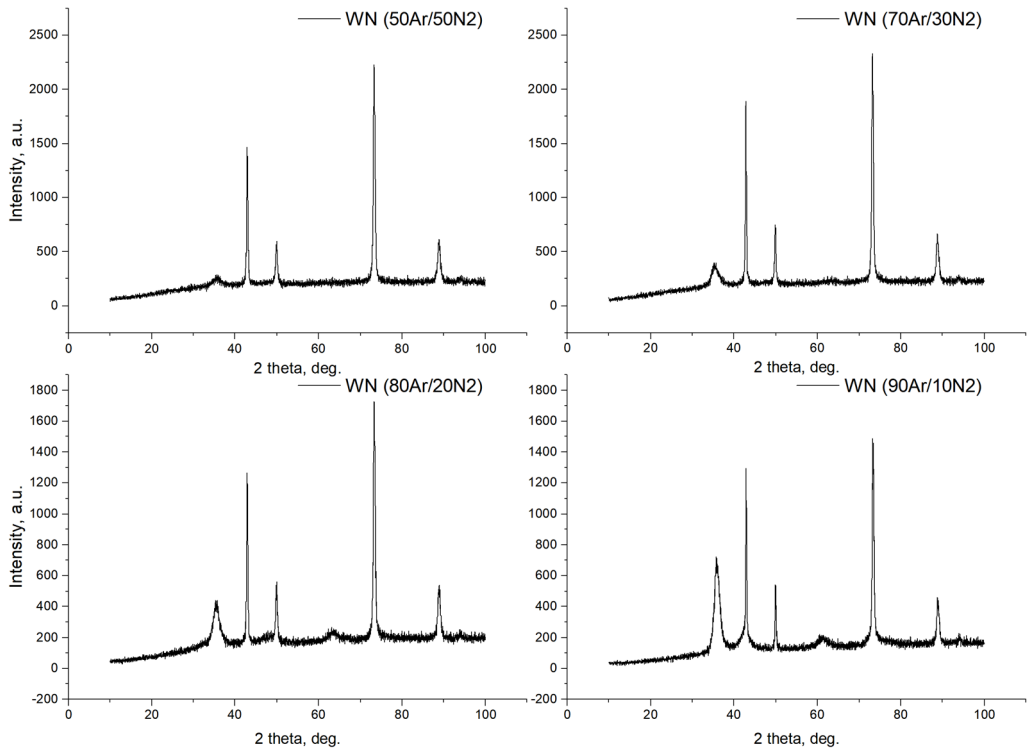

Figure 2. XRD patterns of the WN coatings deposited at different gas regimes

For the WN (80 Ar / 20 N_2) coating, at a nitrogen partial pressure of 20%, the cubic component begins to crystallize more clearly. The intensity of the (111)fcc + (100)hcp reflex doubles compared to the previous regime, reaching the intensity of I/I_0 = 135.23 a.u. Notably, in the mid-angle region of 2theta = 62.54°, the appearance of a combined (220)fcc + (102)hcp phase formation is recorded. This indicates the initiation of structural modification and the rearrangement of

the spatial orientation spectrum of the crystallites under conditions of progressive nitrogen deficiency. This indicates an expansion of the spatial orientation spectrum of the cubic crystallites under conditions of moderate nitrogen deficiency. The texture peak of the hexagonal phase at 2theta = 73.37° remains stable.

For the WN (90 Ar / 10 N_2) coating, under extreme nitrogen deficiency (10%), the phase-structural state of the system undergoes drastic changes. A sharp drop in the intensity of the (200)fcc-W_2N peak to a minimum value of I/I_0 = 49.09 a.u. is recorded, accompanied by a significant increase in its full width at half maximum to FWHM = 1.2000. In parallel, a sharp spike in the intensity of the first peak at 2theta = 35.88° up to I/I_0 = 415.78 a.u. occurs. In the mid-angle region of 2theta = 62.40°, the doublet of the (220)fcc + (102)hcp planes becomes still integrated into the structural matrix. The development of the (101)hcp-WN reflex at 2theta = 49.98° reaches its maximum I/I_0 = 611.13 a.u..

Summarizing the obtained data allows establishing a fundamental relationship between the partial pressure of the reactive gas N_2 and the phase formation kinetics in the W-N system during magnetron sputtering.

Throughout the investigated range of nitrogen concentrations (10% ÷ 50%), the framework of the coatings remains the highly textured hexagonal hcp-WN phase with a preferred orientation of the (111) crystallographic planes. The constancy of the full width at half maximum of this peak FWHM = 0.4800 and the stability of the interplanar spacing d = (1.289 ÷ 1.291) Å indicate that the average size of the coherent scattering domains (grain size) of the hexagonal matrix and its macrostrain level remain invariant to the gas mixture composition in this specific system configuration. However, the dynamics of the accompanying peaks indicate a distinct competition between the growth planes of the cubic fcc-W_2N phase. At high nitrogen flows (30% ÷ 50%), the growth of cubic grains along the (200) axis is energetically more favorable. When the N_2 concentration drops critically to 10%, growth along the (200) direction is heavily suppressed (intensity drops from 622.90 to 49.09 a.u.), with a simultaneous step-like increase in the intensity of the (111)fcc / (100)hcp planes.

The observed substructural effects are explained by changes in the nitrogen saturation degree of the tungsten lattice. In the range of N_2 = (20% ÷ 50%), the high density of the reactive gas ensures an efficient chemical reaction on the substrate, stabilizing the higher nitride phase WN and the ordered semi-nitride phase W_2N with larger, more ordered crystallites (as indicated by the narrow line of the (200)fcc peak with FWHM = (0.3600 ÷ 0.4000). Transitioning to the 20% and 10% N_2 regimes, the chemical reactivity of nitrogen becomes insufficient to complete the phase formation of stoichiometric W_2N along the stable axes. This results in grain refinement (nanocrystallization) of the cubic phase, an increase in lattice microstrains (growth of FWHM to 1.2000 for the (200) plane), and a forced restructuring of the matrix, which manifests as the emergence and integration of the mixed (220)fcc + (102)hcp phase structures.

Thus, varying the composition of the Ar/N_2 gas mixture serves as a precise tool for controlling the ratio between the cubic and hexagonal phases, and allows radically shifting the preferred orientation of the crystallites without degrading the dominant axial (111)hcp-WN texture.

Table 1. Structural-phase data of the WN coatings deposited at different gas regimes (based on XRD patterns presented in Figure 2)

No.	2 theta, deg.	d-spacing, Å	Intensity I/I_0, a.u.	FWHM	Phase	(*hkl*)
WN (50 Ar / 50 N_2)						
1	35.98	-	-	-	fcc-W_2N + hcp-WN	(111) + (100)
2	42.95	2.1040	562.88	0.3600	fcc-W_2N	(200)
3	49.97	1.8236	173.65	0.4800	hcp-WN	(101)
4	73.36	1.2896	1000.00	0.4800	hcp-WN	(111)
5	88.90	1.0999	172.22	0.6800	fcc-W_2N	(400)
WN (70 Ar / 30 N_2)						
1	35.38	2.5349	63.59	1.2800	fcc-W_2N + hcp-WN	(111) + (100)
2	42.86	2.1083	644.97	0.4000	fcc-W_2N	(200)
3	49.90	1.8260	218.83	0.4400	hcp-WN	(101)
4	73.24	1.2913	1000.00	0.4800	hcp-WN	(111)
5	88.83	1.1007	181.84	0.6400	fcc-W_2N	(400)
WN (80 Ar / 20 N_2)						
1	35.42	2.5349	135.23	1.2800	fcc-W_2N + hcp-WN	(111) + (100)
2	42.94	2.1083	622.90	0.4000	fcc-W_2N	(200)
3	49.96	1.8260	202.65	0.4800	hcp-WN	(101)
4	62.54	1.4638	-	-	fcc-W_2N + hcp-WN	(220) + (102)
5	73.37	1.2893	1000.00	0.4800	hcp-WN	(111)
6	88.93	1.0997	199.40	0.6800	fcc-W_2N	(400)
No.	2 theta, deg.	d-spacing, Å	Intensity I/I_0, a.u.	FWHM	Phase	(*hkl*)

No.	2 theta, deg.	d-spacing, Å	Intensity I/I_0, a.u.	FWHM	Phase	(*hkl*)
WN (90 Ar / 10 N_2)						
1	35.88	2.5011	415.78	1.1200	fcc-W_2N + hcp-WN	(111) + (100)
2	42.93	2.1342	49.09	1.2000	fcc-W_2N	(200)
3	49.98	1.8234	611.13	0.4000	hcp-WN	(101)
4	62.40	-	-	-	fcc-W_2N + hcp-WN	(220) + (102)
5	73.37	1.2894	1000.00	0.4800	hcp-WN	(111)
6	88.92	1.0998	201.03	0.6000	fcc-W_2N	(400)

Influence of anode configuration on the structural-phase state

To understand the role of plasma density and ion bombardment kinetics during the deposition process, a comparative analysis was performed on the WN coatings deposited at a fixed gas regime of 80 Ar / 20 N2 under two distinct electrical configurations: an additional biased anode (+200 V) and a grounded anode setup. The respective XRD patterns are shown in Figure 3, and the extracted substructural parameters are listed in Table 2.

A detailed phase and structural evaluation of the individual configurations revealed the following features.

For the WN (80 Ar / 20 N_2) coating with an additional biased anode (+200 V), under the assistance of an additional biased anode, which generates an enhanced glow-discharge plasma zone (plasma density ≈ $7.5 \cdot 10^{10}$ cm^{-3}), the coating stabilizes into a distinct heterophase structure composed of hcp-WN and fcc-W_2N phases. The diffraction profile is dominated by a highly intense and sharp peak at 2theta = 73.37°, corresponding to the (111)hcp-WN plane (I/I_0 = 1000.00 a.u.), FWHM = 0.4800). The cubic phase exhibits a strong preferred growth along the (200)fcc-W_2N plane at 2theta = 42.94° with a high relative intensity of I/I_0 = 622.90 a.u. and a narrow full width at half maximum FWHM = 0.4000. The low-angle combined reflex (111)fcc + (100)hcp at 2theta = 35.42° remains suppressed with intensity of I/I_0 = 135.23 a.u., while a weak, broad features of the mixed (220)fcc + (102)hcp phase assembly is barely traceable in the mid-angle range.

For the WN (80 Ar / 20 N_2) coating with a grounded anode, shifting to the grounded anode configuration, which represents the standard magnetron operation mode without additional plasma enhancement (plasma density ≈ $4 \cdot 10^{10}$ cm^{-3}), induces a profound redistribution of the diffraction intensities. While the dominant texture peak of the hexagonal matrix at 2theta = 73.36° (111)hcp-WN retains its absolute intensity of I/I_0 = 1000.00 a.u, its shape remains unchanged (FWHM = 0.4400). However, a drastic structural rearrangement occurs at lower angles: the combined (111)fcc + (100)hcp peak at 2theta = 36.02° experiences a fourfold intensity spike, rising to I/I_0 = 544.00 a.u. Concurrently, the (200)fcc-W_2N peak at 2theta = 42.95° drops to I/I_0 = 449.85 a.u., and its width broadens slightly to FWHM = 0.4400. Furthermore, a poorly resolved, highly diffused mixed-phase doublet of (220)fcc + (102)hcp becomes clearly visible at 2theta = 62.66°.

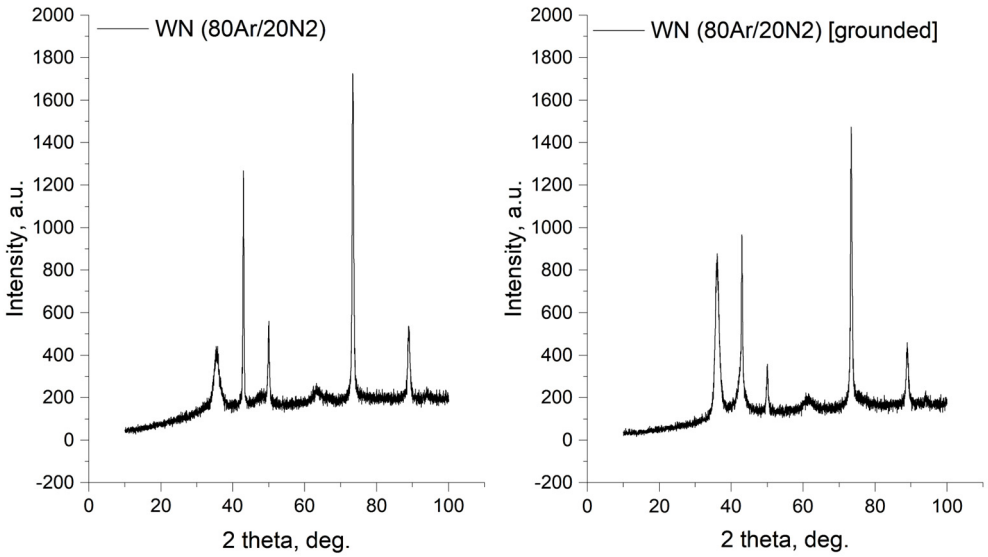

Figure 3. XRD patterns of the WN coatings deposited at 80 Ar and 20 N_2 gas regime and at non- and grounded anodes

The comparative analysis reveals the fundamental physical role of the additional biased anode in governing the phase configuration, texture development, and crystallinity of W-N systems.

1. Ion current density and surface adatom mobility. The primary mechanism driving the structural divergence between the two modes is the alteration of the plasma density near the growth front. When the additional anode is biased at +200 V, it roughly doubles the plasma density of $7.5 \cdot 10^{10}$ cm^{-3} vs. $4 \cdot 10^{10}$ cm^{-3} while maintaining a nearly constant

low ion impact energy of approximately 12 eV. This significant increase in ion flux delivers a continuous supply of low-energy momentum to the surface, effectively accelerating the lateral diffusion of arriving tungsten and nitrogen adatoms without generating structural lattice defects or severe resputtering.

This enhanced adatom mobility provides the system with the activation energy required to overcome local potential barriers, enabling the cubic W_2N phase to crystallize into its thermodynamically preferential orientation along the (200) plane. This is directly manifested in the narrow profile (FWHM = 0.4000) and high intensity of the (200)fcc peak, signaling the formation of larger, highly ordered crystalline domains.

2. Texture randomization and phase degradation via anode grounding. Upon grounding the additional anode, the auxiliary glow discharge is deactivated, causing the local ion current density to drop. Lacking sufficient plasma-assisted energy activation, the surface diffusion length of the adatoms shrinks dramatically. The arriving species are rapidly quenched at or near their landing sites, obstructing the orderly, long-range growth of the cubic lattice along preferred axes.

As a result, the texturing of the cubic component is randomized, leading to the observed deterioration of the (200)fcc growth direction and a dramatic, competitive enhancement of the isotropic (111)fcc + (100)hcp orientation at 2theta = 36.02°. The limitation in diffusion energy also hinders complete chemical phase separation, which promotes the growth of disordered, poorly crystalline interstitial networks. This directly accounts for the broadening of the existing peaks (FWHM) increases from 0.4000 to 0.4400 and the clear emergence of the highly distorted, mixed (220)fcc + (102)hcp phase doublet at 2theta = 62.66°.

In summary, the implementation of an additional biased anode acts as a crucial energetic modifier. It enables precise control over the texture and phase perfection of WN/W_2N nanocomposite coatings by substituting high-energy destructive ion bombardment with high-flux, low-energy plasma activation.

Table 2. Structural-phase data of the WN coatings deposited at different gas regimes (based on XRD patterns presented in Figure 3)

No.	2 theta, deg.	d-spacing, Å	Intensity I/I_0, a.u.	FWHM	Phase	(*hkl*)
WN (80 Ar / 20 N_2)						
1	35.42	2.5349	135.23	1.2800	fcc-W_2N + hcp-WN	(111) + (100)
2	42.94	2.1083	622.90	0.4000	fcc-W_2N	(200)
3	49.96	1.8260	202.65	0.4800	hcp-WN	(101)
4	62.54	1.4638	-	-	fcc-W_2N + hcp-WN	(220) + (102)
5	73.37	1.2893	1000.00	0.4800	hcp-WN	(111)
6	88.93	1.0997	199.40	0.6800	fcc-W_2N	(400)
WN (80 Ar / 20 N_2) [grounded anode]						
1	36.02	2.4914	544.00	1.1200	fcc-W_2N + hcp-WN	(111) + (100)
2	42.95	2.1042	449.85	0.4400	fcc-W_2N	(200)
3	50.00	1.8228	147.08	0.5200	hcp-WN	(101)
4	62.66	-	-	-	fcc-W_2N + hcp-WN	(220) + (102)
5	73.36	1.2896	1000.00	0.4400	hcp-WN	(111)
6	88.91	1.0998	192.82	0.6400	fcc-W_2N	(400)

4. DISCUSSIONS

The structural-phase evolution of the magnetron-sputtered WN coatings is governed by a complex interplay between the thermodynamic driving forces of chemical synthesis (controlled by nitrogen partial pressure) and the kinetic energy delivered to the growing film surface via ion bombardment (governed by the auxiliary anode configuration).

The persistent dominance of the hexagonal hcp-WN phase with a highly stable (111) texture across all gas flow ratios indicates that this structural matrix acts as a rigid energetically favored framework under the given non-equilibrium deposition conditions. The structural invariance of the hcp phase suggests that excess or deficiency of nitrogen primarily affects the secondary, more compliant cubic phase component.

During standard configuration experiments with high nitrogen concentrations (30%–50% of N_2), the high chemical activity of nitrogen facilitates the formation of stoichiometric cubic W_2N phase domains alongside hcp-WN. The preferential growth of these cubic crystallites along the (200) crystallographic orientation represents the minimizing of surface and strain energy under steady-state adatom diffusion. However, as the system transitions into progressive nitrogen deficiency (10% of N_2), the severe restriction of reactive species disrupts the standard nucleation pathways. The growth of the (200) cubic planes becomes heavily suppressed due to the inability to maintain proper stoichiometry along this direction. This induces a state of forced recrystallization and lattice distortion, pushing the cubic matrix towards grain refinement (nanocrystallization) and stimulating the structural integration of mixed-phase structures like the (220)fcc + (102)hcp configurations as a mechanism to accommodate high localized microstrains.

When analyzing the influence of the electrical configuration at a fixed gas regime (80 Ar / 20 N_2), the drastic restructuring observed upon applying the +200 V bias to the additional anode highlights the role of energy transfer at the

film-substrate interface. The biased anode effectively doubles the plasma density (and thus the ion current density) while maintaining a low, non-destructive ion energy profile (~12 eV). From a physical standpoint, this configuration acts as a targeted external energy deliverer that drastically enhances the lateral adatom mobility (surface diffusion length) of arriving W and N species without introducing lattice defects via atomic displacement or resputtering. The accelerated diffusion allows atoms to easily overcome local potential barriers, promoting long-range crystalline ordering and maximizing the crystallization of the thermodynamically stable cubic (200) orientation.

Conversely, when the additional anode is grounded, the auxiliary glow discharge zone collapses, causing a sharp drop in local ion flux. Under these low-flux conditions, arriving adatoms suffer from rapid thermal quenching at or near their immediate landing sites. The restricted surface diffusion prevents the system from undergoing orderly phase separation and structural relaxation. Consequently, the texturing of the cubic component undergoes complete randomization, manifesting as a competitive surge of the isotropic (111)fcc + (100)hcp reflection at 2theta = 36.02°. The lack of plasma-assisted kinetic energy halts the complete chemical synthesis, leading to the accumulation of highly distorted interstitial network boundaries and the emergence of diffused, structurally imperfect mixed-phase configurations. Thus, the auxiliary biased anode serves as an effective tool to decouple the destructive effects of high-energy ion bombardment from the beneficial structural ordering induced by high-flux, low-energy plasma activation.

CONCLUSIONS

In this study, multi-phase tungsten nitride coatings were successfully synthesized under purposefully varied deposition configurations, encompassing a wide range of reactive gas mixture ratios and distinct auxiliary anode connections, specifically tailored to systematically evaluate the competing roles of chemical stoichiometry and low-energy plasma kinetics. Based on the comprehensive structural, phase, and substructural investigation, the following conclusions can be drawn:

1. Magnetron-sputtered tungsten nitride coatings form a complex nanocomposite heterophase structure consisting of a dominant hexagonal hcp-WN phase and a secondary cubic fcc-W_2N phase. The hcp-WN matrix exhibits a rigid, invariant axial growth texture along the (111) crystallographic orientation across the entire investigated range of nitrogen concentrations (10% – 50%).
2. The partial pressure of the reactive gas selectively governs the nucleation kinetics of the compliant cubic phase. High nitrogen contents (30% – 50%) promote orderly growth along the thermodynamically favorable (200)fcc direction. Progressive nitrogen deficiency down to 10% heavily suppresses the (200) growth due to stoichiometry loss, triggering localized microstrains, nanocrystallization, and a forced restructuring into mixed (220)fcc + (102)hcp phase assemblies.
3. The implementation of an auxiliary biased anode (+200 V) doubles the local plasma density to $7.5 \cdot 10^{10}$ cm^{-3} while preserving a non-destructive ion impact energy of approximately 12 eV. This high-flux, low-energy configuration acts as a targeted external energy deliverer that drastically enhances the lateral surface diffusion of arriving W and N adatoms, allowing them to easily overcome potential barriers and form large, highly ordered crystalline domains along the preferred (200) orientation.
4. Operating the system in the standard grounded anode mode (without auxiliary plasma) causes a sharp drop in ion current density. The restricted diffusion energy forces arriving adatoms to undergo rapid thermal quenching at their immediate landing sites, obstructing orderly phase separation. This leads to total texture randomization, a massive fourfold enhancement of the isotropic (111)fcc + (100)hcp peak reflection at 2theta = 36.02°, and the emergence of highly distorted interstitial network boundaries.

Acknowledgments

V.M. Beresnev, I.M. Sereda, Ya.O. Hrechko, A.O. Skrypnyk, S.V. Lytovchenko and B.O.Mazilin were supported by the National Research Foundation of Ukraine in the framework of the project 2025.07/0146.

ORCID

Olga Maksakova, https://orcid.org/0000-0002-0646-6704; **Vyacheslav Beresnev**, https://orcid.org/0000-0002-4623-3243;
Ihor Sereda, https://orcid.org/0000-0002-9111-9853; **Yaroslav Hrechko**, https://orcid.org/0000-0001-9198-3660;
Anatoliy Skrypnyk, https://orcid.org/0009-0004-6863-6563; **Sergiy Bogatyrenko**, https://orcid.org/0000-0002-6044-6886;
Serhiy Lytovchenko, https://orcid.org/0000-0002-3292-5468; **Bohdan Mazilin,** https://orcid.org/0000-0003-1576-0590

REFERENCES

[1] O. Wenzel, V. Rein, M. Hugenschmidt, F. Schilling, C. Feldmann, and D. Gerthsen, RSC Adv. **11**, 28198-28210 (2021). https://doi.org/10.1039/D1RA04448F
[2] H. Liu, Z.-S. Wu, L. Huang, B.-W. Zhang, L.-C. Yin, C.-Y. Xu, and L. Zhen, J. Mater. Chem. A, **9**, 11323-11330 (2021). https://doi.org/10.1039/D1TA01560E
[3] X. Wu, Y. Jiang, T. Wu, B. Zuo, S. Bian, K. Lu, *et al.*, Nanomaterials, **13**, 2205 (2023). https://doi.org/10.3390/nano13152205
[4] Liang, I. Osmond, G. Krach, L.-T. Shi, L. Brüning, U. Ranieri *et al.*, Adv. Funct. Mater. 2313819 (2024). https://doi.org/10.1002/adfm.202313819
[5] S. Anwar, S. Anwar, and B. Priyadarshini, J. Mater. Res. (2024). https://doi.org/10.1557/S43578-024-01353-1
[6] H. Wang, J. Li, K. Li, Y. Lin, J. Chen, L. Gao *et al.*, Chem. Soc. Rev. **50**, 1354-1390 (2021). https://doi.org/10.1039/D0CS00415D

[7] Z. Meng, S. Zheng, R. Luo, H. Tang, R. Wang, R. Zhang, *et al.*, Nanomaterials, **12**, 2660 (2022). https://doi.org/10.3390/nano12152660
[8] Z.-G. Yang, H.-M. Xu, T.-Y. Shuai, Q.-N. Zhan, Z.-J. Zhang, K. Huang, *et al.*, Nanoscale, **15**, 11777-11800 (2023). https://doi.org/10.1039/D3NR01607B
[9] S.K. Mohanty, K.P.K. Reddy, C.-H. Wu, P.-T. Lee, K.-M. Chang, P. Busa, *et al.*, Electronics, **11**, 3432 (2022). https://doi.org/10.3390/electronics11213432
[10] S. Han, S. Yang, X. Zeng, Y. Wu, T. Liu, H. Wang, and S. Ding, Crystals, **14**, 951 (2024). https://doi.org/10.3390/cryst14110951
[11] J. Li, G.-K. Ren, J. Chen, X. Chen, W. Wu, Y. Liu, X. Chen, *et al*., JOM, **74**, 2717-2738 (2022). https://doi.org/10.1007/s11837-022-05294-0
[12] M. Sasani Ghamsari, Metals, **13**, 963 (2023). https://doi.org/10.3390/met13050963
[13] S. Sério, Coatings, **14**, 1041 (2024). https://doi.org/10.3390/coatings14081041
[14] Liang, I. Osmond, G. Krach, L.-T. Shi, L. Brüning, U. Ranieri, *et al*., Adv. Funct. Mater. **34**, 2313819 (2024). https://doi.org/10.1002/adfm.202313819
[15] S. Anwar, S. Anwar, and B. Priyadarshini, J. Mater. Res. (2024). https://doi.org/10.1557/S43578-024-01353-1
[16] L.-C. Chang, M.-C. Sung, L.-H. Chu, and Y.-I. Chen, Coatings, **10**, 1252 (2020). https://doi.org/10.3390/coatings10121252
[17] L. Bana, D. Vavassori, G. Marra, D. Dellasega, and M. Passoni**,** Surf. Coat. Technol. **514**, 132544 (2025). https://doi.org/10.1016/j.surfcoat.2025.132544
[18] Z. Wang, Y. Li, T. Hu, X. Tian, C. Gong, and H. Zhang**,** China Surf. Eng. **38**, 99-106 (2025). https://doi.org/10.11933/j.issn.1007-9289.20240109001
[19] Kosari Mehr, A. Kosari Mehr, Appl. Phys. A, **129**, 693 (2023). https://doi.org/10.1007/s00339-023-06945-y

СТЕХІОМЕТРИЧНА ЕВОЛЮЦІЯ БАГАТОФАЗНИХ НІТРИДІВ ВОЛЬФРАМУ ЗА ЗМІННОГО ПОТОКУ ГАЗУ ТА ВПЛИВУ ДОДАТКОВОЇ ПЛАЗМИ ПІД ЧАС МАГНЕТРОННОГО РОЗПИЛЕННЯ

О.В. Максакова, В.М. Береснєв, І.М. Середа, Я.О. Гречко, А.О. Скрипник, С.І. Богатиренко, С.В. Литовченко, Б.О. Мазілін
Харківський національний університет імені В.Н. Каразіна, майд. Свободи, 4, 61000 Харків, Україна

У роботі систематично досліджено вплив складу газової суміші Ar/N_2 та допоміжної плазмової активації на структурно-фазову еволюцію покриттів нітриду вольфраму (WN), осаджених методом планарного магнетронного розпилення. Покриття синтезували з використанням вольфрамової мішені діаметром 100 мм за різних режимів подачі реактивного газу (від 50 % до 10 % N_2) та за двох електричних конфігурацій: з додатковим зміщеним анодом (+200 В) і зі стандартним заземленим анодом. Результати рентгеноструктурного аналізу в поєднанні з якісною та кількісною оптимізацією показали, що покриття мають складну гетерофазну структуру, утворену гексагональною фазою hcp-WN та кубічною фазою fcc-W_2N. Встановлено, що стійке домінування фази hcp-WN з високо стабільною текстурою (111) відіграє роль жорсткого енергетично вигідного каркаса в усьому діапазоні співвідношень газових потоків. Зменшення вмісту азоту насамперед впливає на вторинний, більш структурно податливий компонент кубічної фази. За критичного дефіциту азоту (10 %) зростання пріоритетно орієнтованих кубічних площин (200) істотно пригнічується, що призводить до подрібнення зерен матриці (нанокристалізації) та стимулює структурну інтеграцію змішаної фазової конфігурації (220)fcc + (102)hcp. Крім того, застосування конфігурації з заземленим анодом призводить до зникнення зони допоміжного тліючого розряду та зниження густини плазми поблизу підкладки з $7{,}5\times10^{10}$ $см^{-3}$ до 4×10^{10} $см^{-3}$. Внаслідок цього скорочується довжина поверхневої дифузії адатомів, що спричиняє швидке термічне загартування структури, повну втрату текстурованості, різке чотириразове зростання інтенсивності ізотропного рефлексу (111)fcc + (100)hcp та накопичення структурно недосконалих міжфазних границь. Застосування допоміжного зміщеного анода є ефективним інструментом для розділення руйнівного впливу високоенергетичного іонного бомбардування та позитивного ефекту структурного впорядкування, індукованого високоінтенсивною низькоенергетичною плазмовою активацією.

Ключові слова: *магнетронне розпилення; нітриди; вольфрам; рентгенівська дифракція; фаза; структура; потік газу*